Natural killer cells' functional impairment drives the immune escape of pre-malignant clones in early-stage myelodysplastic syndromes

A list of authors and their affiliations appears at the end of the paper

Dissecting the preneoplastic disease states' biological mechanisms that precede tumorigenesis can lead to interventions that can slow down disease progression and/or mitigate disease-related comorbidities. Myelodysplastic syndromes (MDS) cannot be cured by currently available pharmacological therapies, which fail to eradicate aberrant hematopoietic stem cells (HSCs), most of which are mutated by the time of diagnosis. Here, we sought to elucidate how MDS HSCs evade immune surveillance and expand in patients with clonal cytopenias of undetermined significance (CCUS), the pre-malignant stage of MDS. We used multi-omic single-cell approaches and functional in vitro studies to show that immune escape at disease initiation is mainly mediated by mutant, dysfunctional natural killer (NK) cells with impaired cytotoxic capability against cancer cells. Preclinical in vivo studies demonstrated that injecting NK cells from healthy donors efficiently depleted CCUS mutant cells while allowing normal cells to regenerate hematopoiesis. Our findings suggest that early intervention with adoptive cell therapy can prevent or delay the development of MDS.

Patients with myelodysplastic syndromes (MDS) have few therapeutic options. At disease onset, almost all hematopoietic stem and progenitor cells (HSPCs) harbor pathogenic genetic alterations[1], suggesting that only allogeneic hematopoietic stem cell transplantation can cure the disease. MDS patients' dismal outcomes could be improved through therapeutic strategies targeting the biological mechanisms underlying the pre-leukemic stage of MDS, clonal cytopenia of undetermined significance (CCUS), which is characterized by reduced clonal burden, lower genetic complexity, and milder peripheral blood (PB) cytopenias[2,3]. In contrast to clonal hematopoiesis of indeterminate potential, a benign age-related condition with a risk of progression to a myeloid malignancy of <1% per year[3], CCUS confers a 5 year cumulative probability of progression to MDS of 82%[2]. This probability exceeds 95% over 10 years if the CCUS clone has a variant allele frequency (VAF) > 20%[2,4]. Thus, there is an unmet need for interventional strategies to prevent or delay the evolution of CCUS to MDS in patients with a high risk of progression.

Deregulated crosstalk between the tumor immune microenvironment and cancer cells leads to tumor immune evasion and is one of the initial causes of cancer formation[5]. During the initial phases of tumor development, the immune system can recognize and eradicate highly immunogenic cancer cells[6]. Still, tumor cells can eventually evade these control mechanisms and escape immune surveillance, thus proliferating and expanding[7,8].

Here, we show how immune evasion affects the initiation of MDS. We demonstrate that among immune system cells, NK cells directly derived from mutant hematopoietic stem cells (HSCs) undergo premature terminal differentiation, which lead to their exhaustion and reduced cytotoxic capability against tumor cells through epigenetic reprogramming that impairs their function.

✉ e-mail: mdaher@mdanderson.org; scolla@mdanderson.org

Results

Immune cells are activated in patients with CCUS

To dissect the molecular mechanisms that enable aberrant HSPC clones to escape immune surveillance, we first transcriptionally profiled the bone marrow (BM) immune microenvironment in patients with CCUS. Single-cell RNA sequencing (scRNA-seq) analysis showed

that, compared with those from young healthy donors (yHDs) and elderly healthy donors (eHDs) (Fig. 1A, Supplementary Fig. 1A, and Supplementary Data 1), BM mononuclear cells (MNCs) isolated from CCUS patients had higher frequencies of natural killer (NK) cells, CD8+ memory cells, and effector memory T cells (Fig. 1B). Differential expression analyses revealed that, compared with those from eHDs,
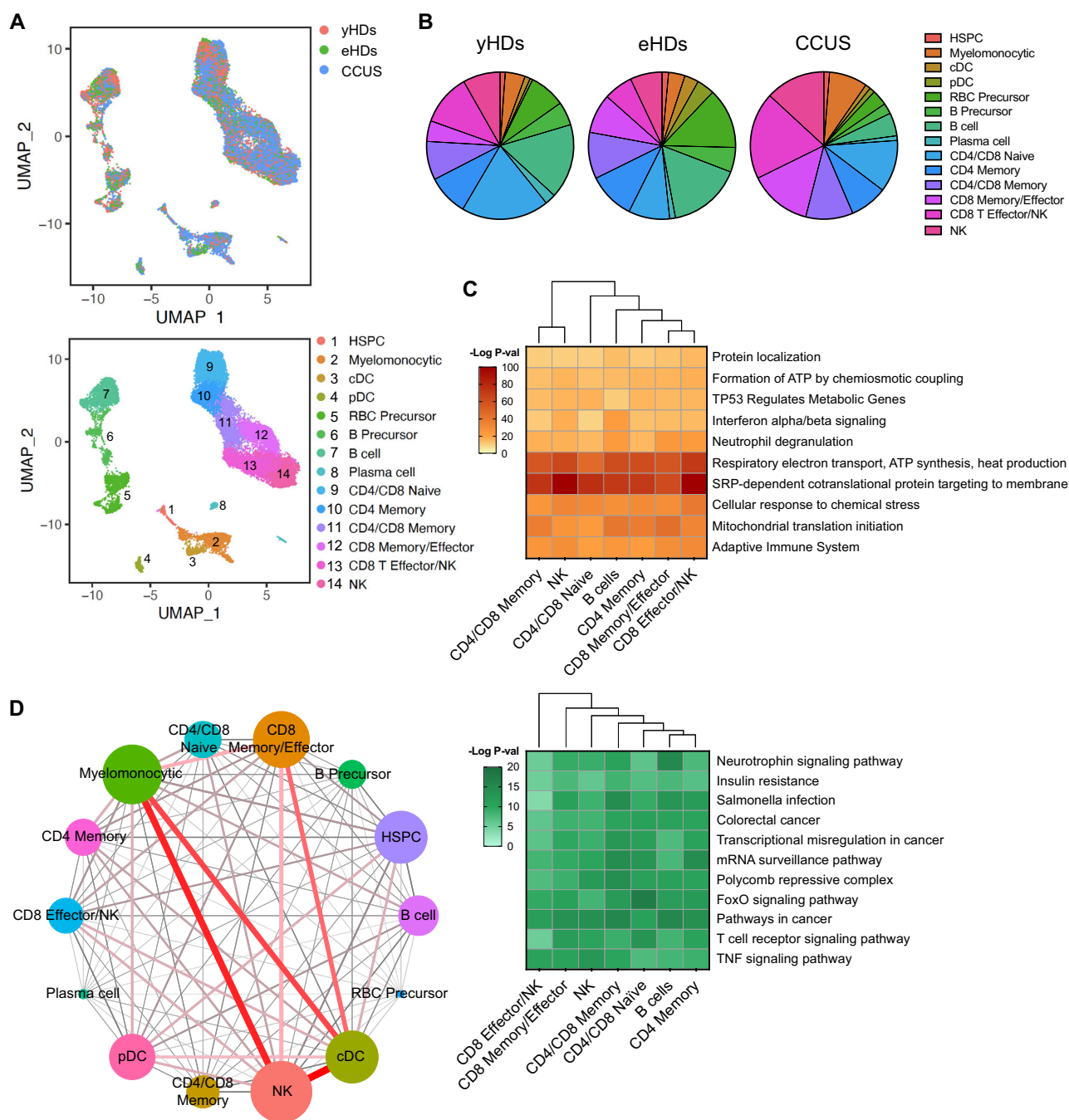

Fig. 1 | **Immune cells are activated in patients with CCUS. A** UMAP plots of scRNA-seq data from BM MNCs isolated from 2 yHDs ($n = 6,494$), 2 eHDs ($n = 3,719$), and 3 patients with CCUS ($n = 11,981$). Each dot represents one cell. Numbering and/or colors represent the sample origin (top) and cell identity (bottom). HSPC, hematopoietic stem and progenitor cell; cDC, classic dendritic cell; pDC, plasmacytoid dendritic cell; RBC, red blood cell. **B** Frequencies of different cell subsets in BM MNCs from yHDs, eHDs, and CCUS patients were analyzed using scRNA-seq. Colors are coded as in **A**, and cell populations are organized in the same order as in the legend, in a clockwise direction. **C** Pathway enrichment analysis of genes that were significantly (P adj ≤ 0.05) upregulated (top) or downregulated (bottom) in

immune cell subsets from CCUS patients compared with those from eHDs. The top 10 Reactome or KEGG gene sets are shown, respectively. **D** Connectome web analysis of interacting MNC types isolated from the BM of CCUS patients compared with those isolated from the BM of eHDs and yHDs. The vertex size is proportional to the number of CCUS-specific interactions to and from each cell type, and the thickness of each connecting line is proportional to the number of interactions between two nodes. A one-sided permutation test was used to determine if a pair was significant. HSPC, hematopoietic stem and progenitor cell; RBC, red blood cell; pDC, plasmacytoid dendritic cell; cDC, classic dendritic cell. Source data are provided as a Source Data file.

immune cells from CCUS patients had upregulated gene expression programs involved in mitochondrial metabolism, protein processing, and response to interferon (IFN)-α/β signaling, which underscores these cells' activation state. In contrast, CCUS immune subsets had significantly downregulated genes involved in immune regulation and inflammation, a phenotypic signature of hypo-responsiveness to extrinsic stimulation[9] (Fig. 1C).

Inflammatory networks modulate the immune microenvironment and contribute to immune escape[10]. To assess the intercellular cross-talk and communication hubs of different cell types in the BM tumor microenvironment of CCUS patients, we inferred cell-cell communications from the combined expression of multi-subunit ligand–receptor complexes using CellPhoneDB, a repository of ligands and receptors and their interactions[11]. Compared with those from yHD and eHD MNCs, the NK cells, myelomonocytes, classic dendritic cells, and memory/effector CD8+ T cells from CCUS MNCs gained significantly more interactions that involved ligands and receptors that regulate leukocyte migration, such as those between the type 1 chemokines MIP-1α (CCL3), MIP-1β (CCL4), and RANTES (CCL5) and their receptors, or between L-selectin and P-selectin ligand (Fig. 1D and Supplementary Figs. 1B, C). These interactions are consistent with the recruitment and migration of NK and effector CD8+ T cells to tumor sites[12,13] and these cells' immune priming by antigen-presenting cells[14,15]. NK and CD8+ T cells from CCUS patients also gained co-stimulatory interactions involving lymphocyte-specific protein tyrosine kinase (LCK) and CD8 or CD58 and CD2, suggesting that these cells initiated an anti-tumoral immune response. Consistent with this hypothesis, multiplex immunofluorescence analysis showed that CD3−CD56+ NK cells were localized near CD33+ myeloid cells and CD3+CD8+ T lymphocytes (Supplementary Fig. 1D). However, other significantly increased cell interactions were predicted to inhibit NK cell function (e.g., through the ligand-receptor pairs HLA-F−KLRC1 and HLA-F−KIR3DL2)[16,17], induce NK tolerance (e.g., through increased CD244 expression in CD8+ T cells, HSPCs, and cDCs, and CD48 expression in NK cells)[18–20], or immunosuppress effector memory CD8+ T cells (e.g., through TGFB/TGFBR1 interactions)[21] (Supplementary Fig. 1C and Supplementary Data 2).

NK cells from patients with CCUS are dysfunctional

Consistent with immune activation–induced proliferation, transcriptional reprogramming, and differentiation toward the acquisition of effector functions[22], additional scRNA-seq analysis of sorted T and NK cells (Supplementary Figs. 2A–C) followed by CytoTRACE (Cellular [Cyto] Trajectory Reconstruction Analysis using gene Counts and Expression; a computational method that predicts cell differentiation states) showed that, compared with those from yHDs and eHDs, CD4+ T, CD8+ T, and NK cells from CCUS patients were in a state of advanced differentiation (Fig. 2A and Supplementary Fig. 2D). Notably, CCUS T and NK cells had significantly downregulated genes involved in the FOXO signaling pathway, including the master regulator *FOXO1*, which is essential for maintaining the quiescent memory state that allows immune cells to respond to and differentiate in response to antigen challenge[23–25] (Supplementary Figs. 2E, F). In line with sustained proliferation and terminal differentiation, CCUS NK cells and CD8+ T cells, but not CD4+ T cells, also had significantly upregulated cell exhaustion markers, including the inhibitory receptors *KLRG1, TIGIT, LAG3*, and *CD160*, which could be correlated with these cells' functional impairment (Fig. 2B). Flow cytometry further validated this exhaustion transcriptional profile at the proteomic level (Supplementary Fig. 2G). Indeed, the IFN-γ secretion capability of CD8+ T cells isolated from the BM of CCUS patients upon tumor cell challenge was significantly decreased compared with that of CD8+ T cells from eHDs, but it was preserved upon T cell receptor–independent stimulation with phorbol 12-myristate 13-acetate and ionomycin (Fig. 2C). These results

confirmed our previous hypothesis that CCUS CD8+ T cells are hypo-responsive to antigen stimulation.

Furthermore, scRNA-seq analysis of NK cells (Supplementary Fig. 2H) showed that CCUS NK cells had a transcriptomic profile enriched in markers of cytotoxic activity, a signature resembling that of the recently defined NK1 subset[26] (Supplementary Figs. 2I, J). Specifically, CCUS NK cells had significantly upregulated MYC and mTOR targets and genes enriched in oxidative metabolism, protein synthesis, and immune signaling (Supplementary Fig. 2K and Supplementary Data 3). During NK cell stimulation, the mTOR-induced post-translational activation of c-MYC triggers metabolic rewiring and protein translation to support NK cells' proliferation burst[27,28], which suggests that CCUS NK cells are hyperactivated. However, compared with eHD NK cells, CCUS NK cells had impaired IFN-γ secretory capacity (Fig. 2D). While CCUS NK cells expressed normal levels of granzyme and lysosome-associated membrane protein 1 (LAMP1; also known as CD107a), which are critical markers of NK degranulation, they also expressed significantly less perforin (Supplementary Figs. 2L, M), a critical cytotoxic protein essential for NK cell killing efficacy[29].

Furthermore, CCUS NK cells challenged with tumor cells showed significantly decreased surface expression of the co-activating receptor CD16 (Fig. 2E) owing to its increased shedding (Supplementary Fig. 2N). CD16, a crucial mediator of target cell death, enables the efficient formation of stable immune synapses and polarized degranulation[30,31] and is essential for NK cell–mediated antibody-dependent cellular cytotoxicity[32]. Indeed, CCUS NK cells' cytolytic capacity against leukemic cells was persistently significantly impaired (Fig. 2F) and was not rescued by culture with K562-based feeder cells in the presence of interleukin (IL)-2 or IL-15 ex vivo (Supplementary Fig. 2O). Moreover, CCUS NK cells had significantly decreased cytotoxicity against allogeneic CCUS CD34+ cells compared with HD NK cells (Fig. 2G), demonstrating that they cannot eliminate premalignant cells. As expected, HD NK cells could not eliminate autologous HD CD34+ cells (Supplementary Fig. 2P).

Mutations in MDS driver genes induce CCUS NK cell dysfunction

Consistent with NK cells' persistent dysfunction, high-throughput single-cell targeted DNA and surface protein sequencing analysis using the Mission Bio Tapestri Platform showed that, independently of the genetic alterations, NK cells isolated from five CCUS patients were part of the mutant clone population and had a clonal burden similar to that detected in myeloid cells (Fig. 3A and Supplementary Figs. 3A, B). However, our in vitro assays had shown a loss of tumor-killing capability beyond what the corresponding VAF of each sample would predict (Figs. 2F, G; Supplementary Figs. 2O, P; Supplementary Data 1), suggesting that the entire NK cell population in CCUS patients is functionally compromised. To dissect the functional state of CCUS NK cells that do not harbor genetic aberrations, we performed long-read scRNA-seq analysis of total BM MNCs from CCUS patients and eHDs. We compared the transcriptional profile of non-mutant NK cells from CCUS patients with that of mutant NK cells from the same CCUS patients and with that of NK cells from eHDs (Fig. 3B and Supplementary Figs. 3C, D). Notably, compared with NK cells from eHDs, non-mutant NK cells from CCUS patients had significantly upregulated genes involved in immune activation (Supplementary Fig. 3E) but downregulated genes associated with NK cell cytotoxicity (Supplementary Fig. 3F and Supplementary Data 4), which suggests a decreased cytotoxic capability of the overall NK cell population. Compared with their CCUS non-mutant counterparts, CCUS mutant NK cells had significantly downregulated genes involved in effector immune functions, such as those regulating cytokine and the Rho GTPase signaling pathways that are essential for immune synapse formation[33] (Fig. 3C and Supplementary Data 5). Given that the cytolytic capability of NK cells isolated from CCUS patients was not rescued
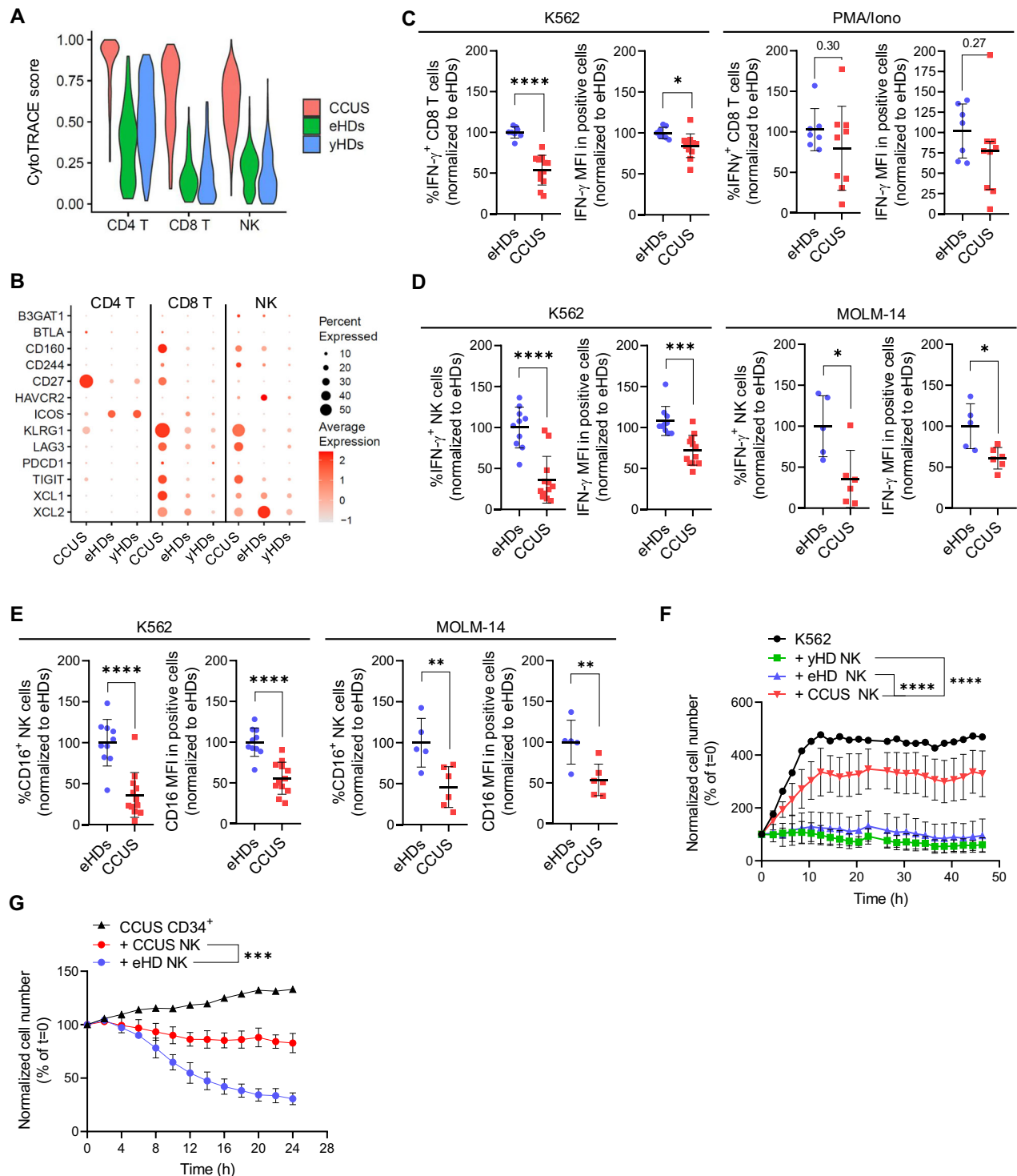
by culture ex vivo, these results suggest that cell-extrinsic mechanisms such as epigenetic rewiring can affect these cells' function.

To evaluate whether *DNMT3A* or *TET2* loss-of-function mutations, which were the most frequent in our cohort of CCUS patients (73%) (Supplementary Data 1)[34], affect NK cells' cytotoxic capability in a cell-autonomous manner, we used CRISPR/Cas9 genome editing to delete *DNMT3A* or *TET2* in healthy NK cells (Supplementary Fig. 3G). *DNMT3A*- or *TET2*-depleted NK cells showed a significant progressive loss of cytolytic capacity following tumor rechallenge, demonstrating that the loss of DNMT3A or TET2 activity is a direct cause of NK cell dysfunction in the context of sustained immune activation (Fig. 3D and Supplementary Fig. 3H). *DNMT3A*- or *TET2*-depleted NK cells isolated after five

tumoral rechallenges had significantly downregulated genes involved in vesicle trafficking, cell cycle, and Rho GTPase signaling processes (Fig. 3E, Supplementary Fig. 3I, and Supplementary Data 6), which is consistent with our observation in CCUS mutant NK cells. NK cells with deficient Rho GTPase signaling lose cytotoxic capacity against target cells owing to impaired actin polymerization and subsequent lytic synapse formation[35]. Indeed, the formation of immune synapses between NK cells and acute myeloid leukemia (AML) cells was significantly impaired by depleting *DNMT3A* or *TET2* in NK cells, as shown by reduced F-actin polymerization and perforin polarization at the synaptic sites (Supplementary Figs. 3J, K). To further dissect the molecular mechanisms underlying NK cells' dysfunction after *DNMT3A*

Fig. 2 | NK cells from patients with CCUS are dysfunctional. A Differentiation scores of CD4+ T, CD8+ T, and NK cells from CCUS patients compared with those from eHDs and yHDs. **B** Normalized expression levels of exhaustion markers in CD4+ T, CD8+ T, and NK cells from CCUS patients, eHDs, and yHDs. **C** IFN-γ expression in CD8+ T cells from eHDs or CCUS patients after stimulation with K562 cells (left; $n = 8$ and $n = 12$, respectively) or phorbol myristate acetate/ionomycin (PMA/Iono; right; $n = 7$ and $n = 9$, respectively). The IFN-γ+ CD8+ T cell frequency and the median fluorescence intensity (MFI) of IFN-γ in CD8+ T cells are shown. Lines represent the mean ± standard deviation. Statistical significance was calculated using unpaired two-tailed t-tests. *$P < 0.05$; ****$P < 0.0001$. K562, IFN-γ MFI in IFN-γ+: $P = 0.0113$. **D** IFN-γ expression in NK cells from eHDs or CCUS patients after stimulation with K562 cells (left; $n = 10$ and $n = 12$, respectively) or MOLM-14 cells (right; $n = 5$ and $n = 6$, respectively). Lines represent the mean ± standard deviation. Statistical significance was calculated using unpaired two-tailed t-tests. *$P < 0.05$; ***$P < 0.001$; ****$P < 0.0001$. K562, IFN-γ MFI in IFN-γ+: $P = 0.002$. MOLM-14, % IFN-γ: $P = 0.0161$; IFN-γ MFI in IFN-γ+: $P = 0.0124$. **E** CD16 expression in NK cells isolated from eHDs or CCUS patients after stimulation with K562 cells (left; $n = 10$ and $n = 12$, respectively) or MOLM-14 cells (right; $n = 5$ and $n = 6$, respectively). The CD16+ NK cell frequency and the MFI of CD16 in NK cells are shown. Lines represent the mean ± standard deviation. Statistical significance was calculated using unpaired two-tailed t-tests. **$P < 0.01$; ****$P < 0.0001$. MOLM-14, % CD16+: $P = 0.0092$; CD16 MFI in CD16+: $P = 0.0091$. **F** Numbers of live K562 cells during 48 h of incubation alone or in co-culture with NK cells isolated from yHDs ($n = 3$), eHDs ($n = 4$), and patients with CCUS ($n = 4$). Symbols and lines represent the mean ± standard deviation. Statistical significance was calculated using one-way ANOVA of the area under the curve using Tukey's multiple comparisons test. ****$P < 0.0001$.
G Numbers of live CD34+ cells from patients with CCUS during 24 h of incubation alone or in co-culture with allogeneic NK cells isolated from eHDs ($n = 2$) or other patients with CCUS ($n = 4$). Symbols and lines represent the mean ± standard deviation. Statistical significance was calculated using one-way ANOVA of the area under the curve using Tukey's multiple comparisons test. ***$P < 0.001$. CCUS vs eHD: $P = 0.0008$. Source data are provided as a Source Data file.

or *TET2* depletion, we performed an ATAC-seq analysis of healthy NK cells depleted of DNMT3A or TET2 through CRISPR/Cas9 gene editing or Cas9 control NK cells and subjected to five tumor rechallenges. This analysis revealed that the depletion of *DNMT3A* or *TET2* in NK cells significantly modified chromatin accessibility in these cells. We observed 1681 and 1832 increased and 278 and 760 decreased open chromatin peaks in *DNMT3A*- or *TET2*-depleted cells, respectively, compared with Cas9 control cells (Supplementary Data 7 and 8). Further analysis of the transcription factor (TF) motifs enriched in the open chromatin peaks identified the TF BATF as the major regulator driving these changes in both conditions (Supplementary Fig. 3L). These data align with previous studies demonstrating that BATF is a central mediator of NK cell epigenetic dysfunction in AML, affecting NK cells' exhaustion and synapse capabilities[36].

NK cells from HDs efficiently target CCUS mutant cells

To evaluate whether *DNMT3A* or *TET2* loss-of-function mutations impair NK cells' cytotoxic capability in vivo, we generated xenograft models of MDS by transplanting the only MDS cell line available (MDS-L) into recipient NSG-SGM3 (NSGS) mice. One month after transplantation, the mice were randomized into three groups based on BM chimerism and injected with HD-derived NK cells previously edited using the CRISPR/Cas9 strategy to achieve *DNMT3A* or *TET2* depletion (Supplementary Fig. 4A). Mice were euthanized 10 days after NK cell injection and BM and splenic cells were analyzed using flow cytometry. Compared with control mice injected with HD NK cells transfected with Cas9 alone, mice injected with *DNMT3A*- or *TET2*-depleted NK cells had a significantly higher tumor burden, as quantified by analyzing the frequency of human BM and splenic CD45+CD56- cells (Fig. 4A), which was associated with a higher level of PB cytopenias (Fig. 4B). NK cell injection did not significantly affect the mouse body or organ weights[37], which suggests that this therapy was well-tolerated (Supplementary Figs. 4B, C). Notably, mice receiving Cas9-transfected NK cells had a significantly higher survival rate than mice injected with NK cells depleted of either *TET2* or *DNMT3A* (Fig. 4C). This finding indicates that the depletion of *TET2* or *DNMT3A* in NK cells critically compromises these cells' antitumor capability in vivo, thereby reducing the mice's survival.

To test the hypothesis that HD-derived NK cells can target CCUS mutant cells, we transplanted BM MNCs isolated from four CCUS patients carrying different VAFs and types of mutations (Supplementary Data 1) into MISTRG mice, which is the only immunocompromised model that allows robust MDS and healthy BM cell engraftment[38,39]. Four weeks after transplantation, mice received healthy NK cells expressing IL-15 or vehicle only (Supplementary Fig. 4D). Compared with the vehicle-treated mice, those injected with HD NK cells had a significantly lower human BM cell burden (Fig. 4D), which was

associated with improved PB cytopenias, including a significant increase in platelet counts (Supplementary Fig. 4E). Flow cytometry of BM MNCs showed reconstitution of human myeloid, lymphoid, and erythroid hematopoietic lineages (Supplementary Fig. 4F, G). Next-generation sequencing (NGS) analysis of human CD45+ cells depleted of mouse CD45+ cells sorted from the BM of two xenografts showed that healthy NK cells could efficiently target mutant cells while sparing their wild-type counterparts (Fig. 4E and Supplementary Data 9). Together, these results demonstrate that CCUS cells are not intrinsically resistant to NK cell–mediated cytotoxicity and suggest that allogeneic NK cells from HDs can efficiently eradicate CCUS mutant cells in vivo, thus preventing tumor progression.

Discussion

The development of strategies to prevent or delay MDS evolution has been hindered by a poor understanding of how mutant cells outcompete their healthy BM counterparts and the scant applicability of mutation-specific studies in the highly genetically heterogeneous MDS patient population. Patients with CCUS at an increased risk of progression to MDS or AML, defined by the cooccurrence of multiple mutations and/or an elevated clonal burden[40], are ideal candidates for mechanistic studies and early intervention approaches.

Given that immune evasion by clonal cells is one of the primary mechanisms of cancer initiation, we first comprehensively analyzed the CCUS immune BM microenvironment at the single-cell resolution. Our single-cell transcriptomic analyses revealed that CCUS NK cells, the initial players in the antitumoral immune response[41], are activated but hyporesponsive and undergo premature terminal differentiation, which leads to these cells' reduced effector function and exhaustion[42]. Functional assays confirmed that CCUS NK cells have decreased IFN-γ secretion, reduced CD16 and perforin expression, and deficient immune synapse formation, directly impairing their cytotoxic capacity against leukemic cell lines and primary CCUS CD34+ HSPCs. Notably, CCUS NK cell dysfunction persisted despite ex vivo recovery attempts, suggesting that cell-autonomous mechanisms mainly drive functional impairment. Indeed, high-throughput scDNA-seq paired with immunophenotypic analysis revealed that CCUS NK cells are enriched in the mutant clone, which suggests that myeloid driver mutations impair NK cell function. This hypothesis was validated by the CRISPR/Cas9-mediated depletion of *DNMT3A* and *TET2* in healthy NK cells, which led to a progressive loss of cytotoxicity, along with the downregulation of genes that are crucial for immune synapse formation and effector function, mimicking the dysfunction observed in CCUS-derived NK cells. Moreover, *DNMT3A*- or *TET2*-depleted NK cells failed to prevent tumor progression in xenograft models, allowing increased malignant cell infiltration in the BM and leading to reduced survival rates in recipient mice. These results align with a previous study showing that
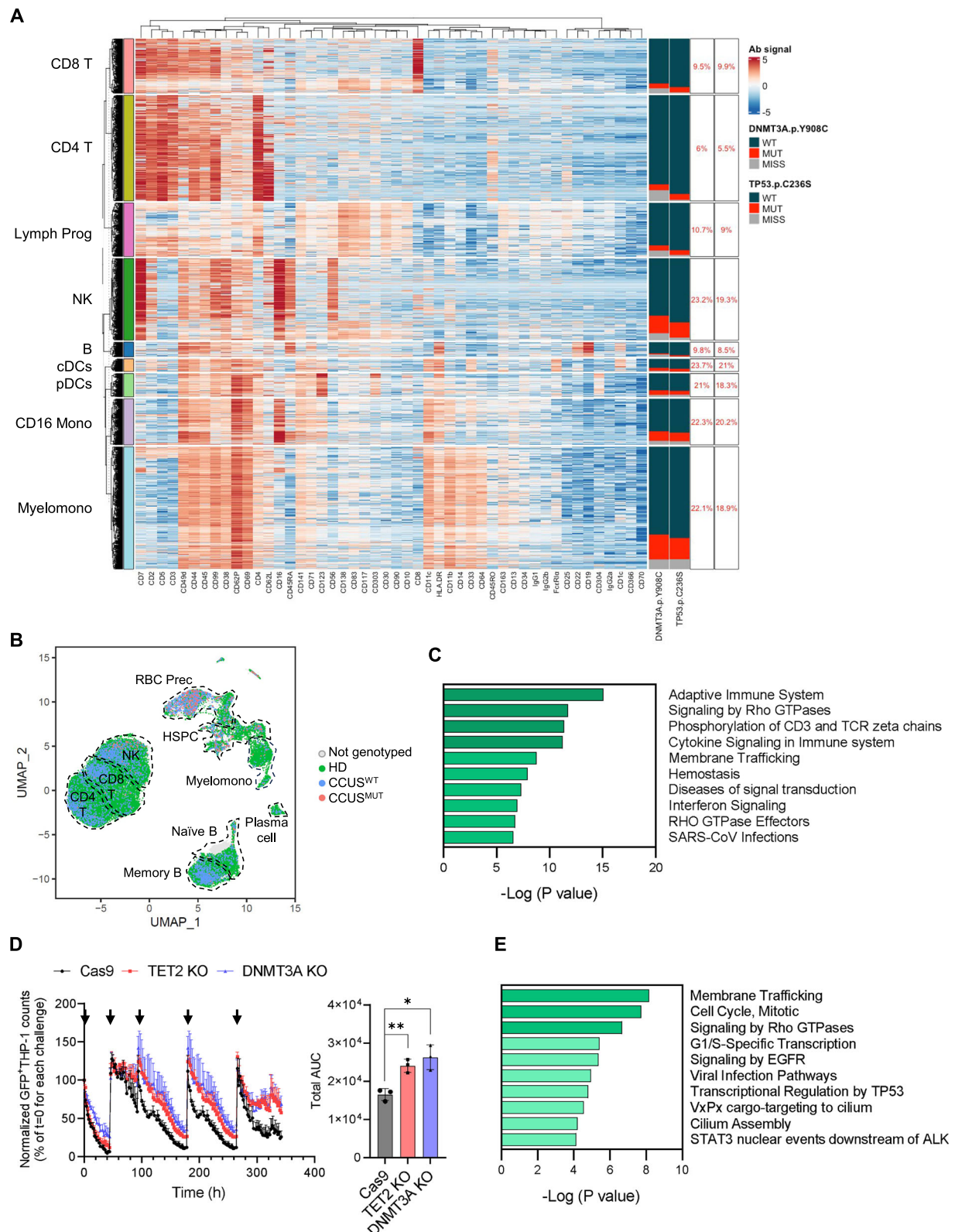
TET2-mutated NK cells from MDS patients exhibit decreased expression of killer immunoglobulin-like receptors, perforin, and TNF-α, promoting disease progression[43].

Our results show that the most frequent MDS driver mutations, such as those affecting *TET2* or *DNMT3A*, induce immune dysfunction at disease initiation, thus enabling the evasion of premalignant clones. Although somatic mutations can intrinsically drive NK cell dysfunction, a significant fraction of NK cells remained unmutated. However, NK cells exhibited a substantial loss of tumor-killing capability (not recovered after in vitro culture) beyond what the mutation VAF would predict. These results suggest that the fitness of wild-type cells is also compromised. Indeed, our long-read scRNA-seq analyses revealed that the transcriptomic signatures of wild-type NK cells from CCUS patients resemble those of mutant NK cells. This observation is consistent with recent findings showing that MDS CD34+ cells harboring a deletion of chromosome 5 and those

Fig. 3 | Somatic mutations in MDS driver genes induce CCUS NK cell dysfunction. A Single-cell genotypes of BM MNCs ($n = 2{,}518$), by immunophenotype, from a representative CCUS patient (CCUS-52) with *DNMT3A* (VAF = 15%) and *TP53* (VAF = 13%) mutations. Each line represents a cell. The heatmap represents antibody signal intensity; each column represents one surface marker. The colored bars to the left of the heatmap represent different cell types based on the antibody intensity. The colors and percentages in the sidebars to the right of the heatmap show each cell type's genotype. Immunophenotypes and genotypes are unaligned. Lymph, lymphoid; Prog, progenitors; cDCs, classic dendritic cells; pDCs, plasmacytoid dendritic cells; Mono, monocytes; Myelomono, myelomonocytic; Ab, antibody; WT, wild type; MUT, mutated; MISS, missing. **B** UMAP plot of long-read scRNA-seq data from BM MNCs isolated from 2 CCUS patients ($n = 52{,}751$) and two eHDs ($n = 52{,}330$). Different colors represent cell identity and genotype. RBC Prec, red blood cell precursors; HSPC, hematopoietic stem and progenitor cell; Myelomono, myelomonocytic. **C** Pathway enrichment analysis of genes that were

significantly downregulated ($P \leq 0.05$) in CCUS mutant NK cells compared to CCUS non-mutant NK cells. The top 10 Reactome gene sets are shown. **D** Number of live THP-1 cells co-cultured with HD NK cells transfected with Cas9 in the absence (Cas9; control) or presence of sgRNAs against *TET2* (*TET2* KO) or *DNMT3A* (*DNMT3A* KO) after 5 rounds of tumor cell challenge (black arrows). The experiment was performed twice using 2 independent guides per gene. Symbols and lines represent the mean ± standard deviation of tumor indexes in three biological replicates from one representative experiment (left) and the corresponding areas under the curve (AUC; right). Statistical significance was calculated using one-way ANOVA of the AUC using Dunnett's multiple comparisons test. *$P < 0.05$, **$P < 0.01$. Cas9 vs *TET2* KO: $P = 0.0067$; Cas9 vs *DNMT3A* KO: $P = 0.0242$. **E** Pathway enrichment analysis of genes that were significantly downregulated (P adj ≤ 0.05) after 5 tumoral challenges in both *TET2*-KO and *DNMT3A*-KO NK cells but not in Cas9 controls. The top 10 Reactome gene sets are shown. Source data are provided as a Source Data file.
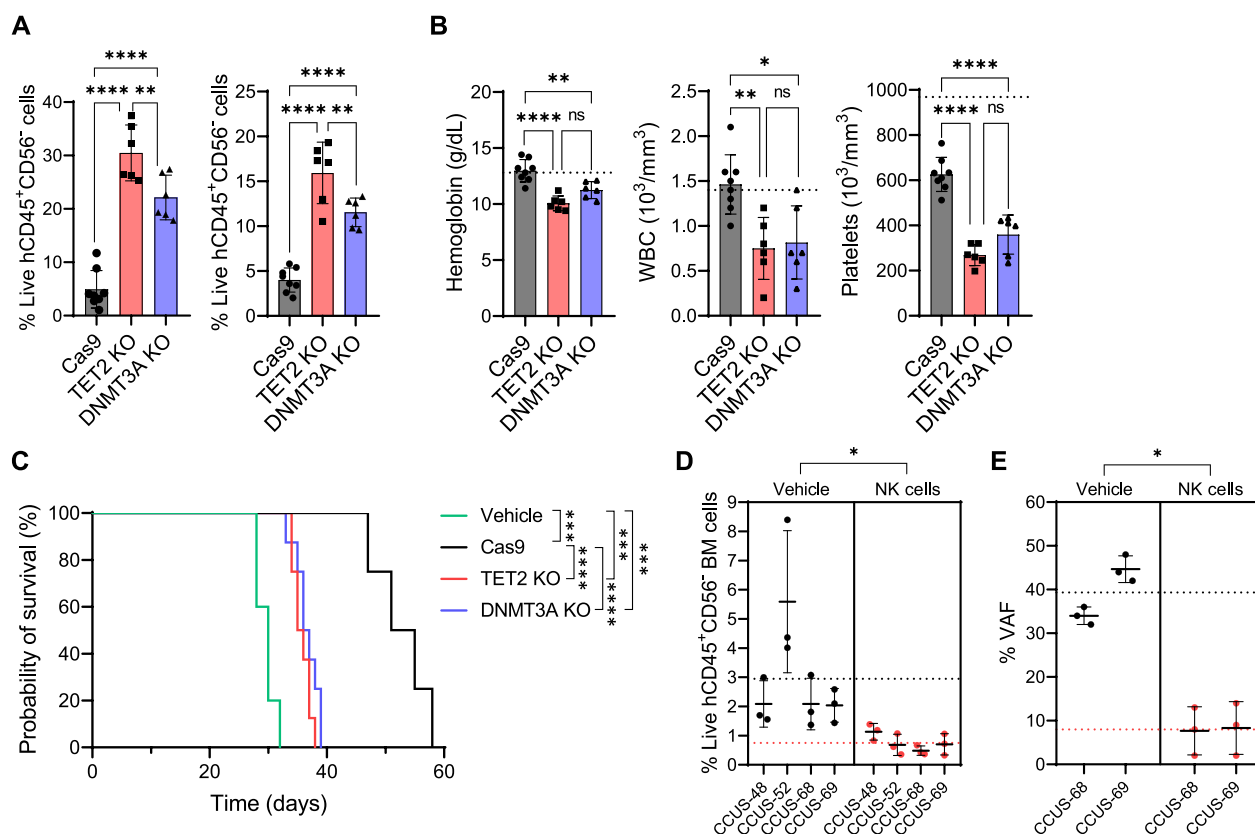

Fig. 4 | NK cells from HDs efficiently target CCUS mutant cells. A Frequencies of MDS-L cells in the BM (left) and spleen (right) of engrafted NSGS mice 10 days after the injection of NK cells transfected with Cas9 in the absence (Cas9; $n = 8$) or presence of sgRNAs against *TET2* (TET2 KO; $n = 6$) or *DNMT3A* (DNMT3A KO; $n = 6$). Statistical significance was calculated using one-way ANOVA and Tukey's multiple comparisons test. **$P < 0.01$, ****$P < 0.0001$. BM, *TET2* KO vs *DNMT3A* KO: $P = 0.0035$; spleen, *TET2* KO vs *DNMT3A* KO: $P = 0.0084$. hCD45, human CD45. Error bars represent the mean ± standard deviation. **B** PB blood counts in engrafted NSGS mice 10 days after the injection of NK cells transfected with Cas9 ($n = 8$) in the absence or presence of sgRNAs against *TET2* ($n = 6$) or *DNMT3A* ($n = 6$). Dotted lines represent the mean of hemoglobin, white blood cell counts, and platelets for 8 week-old NSGS mice based on the Mouse Phenome Database (Jackson Laboratories). Statistical significance was calculated using one-way ANOVA and Tukey's multiple comparisons test. *$P < 0.05$, **$P < 0.01$, ****$P < 0.0001$. Hemoglobin, Cas9 vs *DNMT3A* KO: $P = 0.004$; *TET2* KO vs *DNMT3A* KO: $P = 0.0651$. White blood cells (WBC), Cas9 vs *TET2* KO: $P = 0.005$; Cas9 vs *DNMT3A* KO: $P = 0.0103$; *TET2* KO vs *DNMT3A* KO: $P = 0.9445$. Platelets, *TET2* KO vs *DNMT3A* KO: $P = 0.1041$. Error bars represent the mean ± standard deviation. **C** Kaplan–Meier survival analysis of NSGS mice transplanted with MDS-L cells injected with vehicle ($n = 5$) or NK cells

transfected with Cas9 in the absence ($n = 8$) or presence of sgRNAs targeting *TET2* ($n = 8$) or *DNMT3A* ($n = 8$). Statistical significance was calculated using a log-rank (Mantel-Cox) analysis adjusted by Holm's multiple comparisons test. ***$P < 0.001$. Vehicle vs Cas9: $P = 0.0002$; Vehicle vs *TET2* KO: $P = 0.0002$; Vehicle vs *DNMT3A* KO: $P = 0.0002$; *TET2* KO vs *DNMT3A* KO: $P = 0.2036$. **D** Frequencies of human CD45$^+$CD56$^-$ cells in the BM of MISTRG mice transplanted with cells from 4 patients with CCUS. Samples were analyzed 1 week after the injection of vehicle ($n = 3$/each) or HD NK cells ($n = 3$/each). Dotted lines are color-coded and represent the mean of each group. Statistical significance between treatment groups was calculated using a two-tailed nested *t*-test. *$P < 0.05$. Vehicle vs NK cells: $P = 0.0486$. Error bars represent the mean ± standard deviation. **E** VAF in mouse CD45-depleted and human CD45-enriched BM cells isolated from MISTRG donor mice transplanted with cells from 2 CCUS patients 1 week after the injection of vehicle ($n = 3$/each) or healthy NK cells ($n = 3$/each). Dotted lines are color-coded and represent the mean of each group. Statistical significance between treatment groups was calculated using a two-tailed nested *t*-test. *$P < 0.05$. Vehicle vs NK cells: $P = 0.0279$. Error bars represent the mean ± standard deviation. Source data are provided as a Source Data file.

without the deletion in the same patient displayed similar transcriptional alterations[44].

Loss-of-function alterations affecting *TET2* and *DNMT3A* may have distinct effects on immune cells. Recent findings have shown that *TET2*-deficient chimeric antigen receptor (CAR) T cells exhibit an abnormal epigenetic landscape, functional changes characterized by the heightened production of TNF-α, IL-2, and IL-6 upon stimulation, and an increased cytotoxic profile[45]. *DNMT3A* depletion increases CAR T cells' proliferative capability without inducing the typical exhaustion phenotype acquired upon chronic stimulation[46,47]. However, our single-cell targeted DNA and surface protein sequencing analysis using the Mission Bio Tapestri platform demonstrated that the frequency of mutated T cells in CCUS is low, which is consistent with NK cells and T cells having different ontologies.

Our findings have important translational implications. Emerging therapies for MDS, such as venetoclax-based therapies or agents targeting driver mutations, show promise but have yet to significantly improve the dismal prognosis of these patients, possibly owing to the high mutational burden at diagnosis. Thus, future therapeutic efforts should prioritize early intervention in CCUS when the mutational burden is lower and symptoms are less severe.

The lack of a standard of care for high-risk CCUS patients, despite these patients' recurrent transfusion dependency, underscores the urgent need for targeted therapies. Our results suggest a therapeutic window for immune therapies in this subset of patients. Promising approaches may include adoptive cell therapies based on allogeneic NK cells or CAR NK cells, which are currently being evaluated in relapsed/refractory AML and MDS[48,49]. These therapies have the added advantage of not being dependent on the target MDS stem cells' genotype or phenotype, both of which play a role in the resistance to current therapies[50,51].

The safety of any cell-based therapeutic intervention is paramount, particularly for patients with conditions like CCUS, for whom the clinical significance and expected benefits of cell-based therapies remain an area of active investigation. CAR NK cells derived from allogeneic sources, such as cord blood, have a strong safety profile. Unlike CAR T cells, CAR NK cells have not been associated with graft-versus-host disease in the allogeneic setting, and clinical studies of CAR NK cells have not shown cytokine release syndrome[52,53]. The shorter lifespan of NK cells relative to T cells, combined with the host's natural rejection of allogeneic cells, further enhances the safety of CAR NK cells, as they do not persist long-term in the body. Additionally, the incorporation of safety switches, such as inducible caspase 9, can be activated to eliminate the cells if any adverse effects occur. Using cells from HD sources, such as cord blood, also poses a lower risk of malignant transformation than cells derived from patients with malignancy. Nonetheless, as with all gene-modified cell therapies, long-term monitoring remains essential to assess potential delayed effects. However, based on existing clinical data, we emphasize that the excellent safety profile of CAR NK cells, mainly those from allogeneic HD sources, supports their potential as a safer alternative among adoptive cell therapies.

In conclusion, our findings uncover early dysfunction in NK cells, opening potential therapeutic avenues to prevent or arrest progression to MDS and its severe outcomes.

Methods

The research complies with all relevant ethical regulations: MD Anderson Cancer Center IRB-approved human sample protocol PA15-0926; MD Anderson Cancer Center IACUC-approved mouse protocol 0000931-RN03.

Primary human specimens

BM aspirates from five yHDs (median age = 23 years) and 22 eHDs (median age = 55 years) were obtained from Lonza (Morristown, NJ) and AllCells (Alameda, CA) or the Department of Stem Cell Transplantation and Cellular Therapy at MD Anderson Cancer Center (Supplementary Data 1). BM aspirates and PB samples from 30 CCUS patients (median age = 72.5 years) were obtained from the Department of Leukemia at MD Anderson and the Department of Medicine at the University of California San Diego (Supplementary Data 1). BM biopsy samples from seven CCUS patients (median age = 65 years, 57% male) were obtained from the Department of Hematopathology at MD Anderson. HD NK cells were isolated from cord blood donor units for research use provided by the MD Anderson Cord Blood Bank. All samples were obtained following the Declaration of Helsinki and with the approval of the corresponding Institutional Review Boards. Written informed consent was obtained from all donors. No compensation was provided to the study participants.

We did not perform sex- or gender-based analyses. Patient samples were selected based on diagnosis regardless of sex and gender. Males and females had comparable distributions in the CCUS and HD cohorts. Gender is not relevant to this study. The sex of all patients in each experiment is included in Supplementary Data 1. Due to the limited number of subjects in each experiment, disaggregated analysis by sex can not be performed.

CCUS patient diagnoses were performed by a hematologist and confirmed by a dedicated pathologist. Patients' genomic information was assessed by NGS performed in Clinical Laboratory Improvement Amendments–certified laboratories at the corresponding institutions as described previously[54]. None of the CCUS patients received therapy during the sample collection. MNCs were isolated from each BM sample using the standard gradient separation approach with Ficoll-Paque PLUS (GE Healthcare Lifesciences).

Cell lines

K562 and THP-1 cells were purchased from ATCC (CCL-243 and TIB-202, respectively), and MOLM-14 cells were purchased from DSMZ (ACC 777). The MDS-L cell line, established from a male MDS patient, was a generous gift from Dr. Kaoru Tohyama (Department of Laboratory Medicine, Kawasaki Medical School, Okayama, Japan). K562-based feeder cells were retrovirally transduced to co-express 4-1BBL, CD48, and membrane-bound IL-21a[55]. The identity of the cell lines was confirmed by short tandem repeat DNA fingerprinting at MD Anderson's Cytogenetics and Cell Authentication Core.

Fluorescence-activated cell sorting

For the scRNA-seq analysis of total BM, MNCs were stained with 4′,6-diamidino-2-phenylindole (DAPI), and live cells were purified by fluorescence-activated cell sorting (FACS). For the scRNA-seq analyses of T and NK cells, CD3+ T and CD56+ NK cells were sorted using DAPI and antibodies against human CD3 (SK7, 1:10) and CD56 (B159, 1:40). FACS was performed in a BD Influx Cell Sorter (BD Biosciences). The cell populations were gated and acquired using FACSDiva software v8.01 (BD Biosciences).

scRNA-seq

scRNA-seq analysis was performed as previously described[50,56]. FACS-purified live BM MNCs or T/NK cell fractions were prepared and sequenced at MD Anderson's Advanced Technology Genomics Core. Sample concentration and cell suspension viability were evaluated using a Countess II FL Automated Cell Counter (Thermo Fisher Scientific) and manual counting. Samples were normalized for input onto the Chromium Single Cell A Chip Kit (10x Genomics, Pleasanton, CA), in which single cells were lysed and barcoded for reverse transcription. The pooled, single-stranded, barcoded cDNA was amplified and fragmented for library preparation. Pooled libraries were sequenced on a NovaSeq 6000 SP 100-cycle flow cell (Illumina, San Diego, CA).

Data were analyzed using 10x Genomics' CellRanger software (version 7.1.0). Fastq files were generated using the CellRanger

mkfastq pipeline (version 7.1.0). Raw reads were mapped to the human reference genome (refdata-cellranger-GRCh38-3.0.0) using the Cell-Ranger count pipeline. The digital expression matrices were analyzed with the R package Seurat (version 4.3.0)[57] to identify different cell types and signature genes for each cell type. Specifically, cells with fewer than 100 genes or greater than 25% mitochondrial expression were removed from further analysis. The Seurat function NormalizeData was used to normalize the raw counts. Variable genes were identified using the FindVariableFeatures function. The ScaleData function was used to scale and center the counts in the dataset. Principal component analysis (PCA) of the variable genes was performed as previously described[56]. The RunHarmony function from the Harmony package was applied to remove potential batch effects among samples processed in different batches[58]. Uniform Manifold Approximation and Projection (UMAP) dimensional reduction was performed using the RunUMAP function. The clusters were obtained using the FindNeighbors and FindClusters functions with a resolution of 0.6. The cluster marker genes were found using the FindAllMarkers function. The cell types were annotated by overlapping the cluster markers with the canonical cell type signature genes[56]. Differential expression analysis between any two groups of cells was carried out using the FindMarkers function. Genes with an adjusted P-value < 0.05 were considered significantly differentially expressed. Pathway analyses of differentially expressed genes were conducted using Metascape[59]. The module scores were calculated using the AddModuleScore function on the intended gene lists. The CytoTRACE score was computed by uploading the expression matrix to the CytoTRACE web tool (https://cytotrace.stanford.edu/)[60].

CellphoneDB (version 3)[11] was applied for ligand-receptor analysis. Each cell type was separated by disease classification (yHD, eHD, or CCUS), and a separate run was performed for each classification. If a cell type contained fewer than 10 cells for a disease classification, it was not considered in the ligand-receptor analysis for that disease classification. Pairs with a P-value > 0.05 were filtered out from further analysis. Each pair was assigned to the condition with the highest interaction score to compare the disease conditions. The number of interactions between each cell-type pair was then calculated. The connectome web was plotted using the R package igraph. The predicted ligand-receptor pairs were further filtered for data interpretation using CellTalkDB and a bibliographic search to select only biologically validated interactions.

Long-read scRNA-seq

BM MNCs from two CCUS patients and two eHDs were assessed for concentration and viability using a Life Technologies Countess 3 FL cell counter and trypan blue exclusion staining. Suspensions with 70% or higher viability were used for capture. Two to five sample suspensions were captured for each sample, targeting 50,000 cells per sample. Single-cell capture was performed on the Chromium iX using 10x Genomics' Next GEM 3' scRNAseq V3.1 protocol (CG000315_ChromiumNextGEMSingleCell3-GeneExpression, v3.1, DualIndex_RevE), up to and including cDNA amplification and cleanup. The purified, amplified cDNA was assessed for quality and concentration using an Agilent HS DNA Bioanalyzer and the Qubit HS dsDNA Assay (both from Thermo Fisher). Ten nanograms of the resultant barcoded, full-length cDNA transcripts were used as templates for Nanopore full-length cDNA library preparation. The transcripts were first amplified with custom biotinylated primers. The resultant biotinylated cDNA was captured following bead cleanup using streptavidin beads. The eluted cDNA was used in a second round of PCR, and the product was used to generate nanopore libraries using the Ligament Sequencing Kit V14 (Nanopore, SQK-LSK114). Purified libraries were quantified using the Qubit HS dsDNA Assay, and 100 fmoles of library were loaded to R10.4.1 flow cells (FLO-PRO114M) and sequenced on a PromethION 24 sequencer. Libraries were sequenced for 72 h with a 200-bp

minimum read length using the super accurate base-calling mode. Single-cell full-length cDNA libraries were prepared using the 10x Genomics microfluidics-based Chromium platform. Subsequently, these libraries underwent sequencing on a Nanopore PromethION Flow Cell. Each PromethION Flow Cell typically yields ~80 million cell-assigned reads, allowing for the analysis of up to around 8000 cells per flow cell. Multiple libraries were prepared from the same sample to ensure an adequate number of cells and achieve a higher sequencing depth, and several sequencing runs were conducted for each library.

The primary data analysis, including barcode and unique molecular identifier demultiplexing, was performed using the EPI2ME software. This workflow generates a gene expression matrix per library, merging these matrices across all libraries. The R package Seurat (v4.3.0) was used to cluster the cells in the merged matrix. Cells with >20% mitochondrial expression were filtered out as low-quality cells. The NormalizeData function was used to normalize the expression level for each cell with default parameters. The FindVariableFeatures function was used to select variable genes with default parameters. The ScaleData function was used to scale and center the counts in the dataset. PCA of the variable genes was performed. The RunHarmony function from the Harmony package was applied to remove the potential batch effect among samples. UMAP dimensional reduction was performed using the RunUMAP function as previously described[61]. The clusters were obtained using the FindNeighbors and FindClusters functions with the resolution set to 0.5. The cluster marker genes were found using the FindAllMarkers function. The cell types were annotated by overlapping the cluster markers with the published marker genes. The genotypes of the cells were called using cb_sniffer, a tool that extends the PySam library to do barcode-aware pileups (https://github.com/sridnona/cb_sniffer). Differential expression analysis between the groups of cells was performed using the FindMarkers function.

Flow cytometry analysis

Cells were stained with the Zombie NIR Fixable Viability Kit, washed twice with Cell Staining Buffer, and incubated with 5 μL of True-Stain Monocyte Blocker and 5 μL of Human TruStain FcX (all from BioLegend). Cells were then washed and incubated with antibodies against the surface markers CD3 (SK7, 1:80), CD4 (SK1, 1:80), CD8 (SK1, 1:80), CD56 (B159, 1:80), CD19 (HIB19, 1:200), CD14 (63D3, 1:80), CD34 (581, 1:10), CD33 (P67.6, 1:80), CD57 (QA17A04, 1:80), CD28 (CD28.2, 1:80), CD244 (C1.7, 1:80), CD27 (O323, 1:80), TIM3 (F38-2E2, 1:80), KLRG1 (SA231A2, 1:80), LAG3 (11C3C65, 1:80), TIGIT (A15153G, 1:80), and PD1 (A17188A, 1:80; all from BioLegend).

To evaluate the reconstitution of human BM after CCUS cell transplantation, we stained BM MNCs with antibodies against mouse CD45 (30-F11, 1:100; BioLegend) and Ter119 (TER-119, 1:25; BioLegend) and against human CD45 (HI30, 1:20; BioLegend), CD34 (581, 1:20; BD Horizon), CD71 (CY1G4, 1:20; BioLegend), CD33 (WM53, 1:20; BioLegend), CD15 (H198, 1:20; BioLegend), CD14 (HCD14, 1:20; BioLegend), and CD19 (HIB19, 1:20; BioLegend).

The cell populations were analyzed using FlowJo software (version 10.7.1). All experiments included single-stained controls.

Multiplex immunofluorescence analysis

BM core biopsy samples were used for multiplex immunofluorescence assessment. We optimized and validated a multiplex immunofluorescence panel using antibodies against CD3e, CD8, CD33, and CD56. Each antibody was assessed by multiplex immunofluorescence using the Opal 9 kit (Akoya Biosciences, Marlborough, MA) with the following clones and dilutions: CD3e (D7A6E, 1:100; Cell Signaling Technology), CD8 (C8/144B, 1:25; Invitrogen), CD56 (123C3, 1:25; Dako), and CD33 (BCL-L-CD33, 1:100; Leica). The slides were imaged using the Vectra Polaris spectral imaging system (Akoya Biosciences). Each marker was analyzed at the single-cell level, and a supervised

algorithm for phenotyping was built for each marker. The cell density for each marker and combinations of phenotypes were consolidated using Spotfire software (TIBCO Spotfire).

Cytokine secretion assays

In T cell assays, BM MNCs were cultured in RPMI medium with 2 mM glutamine and 10% fetal bovine serum (FBS) in the presence of brefeldin A and were stimulated with K562 cells at a 1:1 effector:tumor (E:T) ratio or with PMA/ionomycin (Leukocyte Activation Cocktail with GolgiPlug, BD Biosciences) for 4 h at 37 °C and 5% CO_2. In NK cell assays, NK cells isolated from BM MNCs by negative magnetic selection using the NK Cell Isolation Kit (Miltenyi Biotec) were cultured in a 1:1 mix of Click's media: RPMI media and stimulated with K562 cells (1:1 E:T) for 4 h in the presence of brefeldin A at 37 °C and 5% CO_2. After incubation, MNCs or NK cells were harvested, washed with phosphate-buffered saline (PBS), and stained with the viability dye Zombie UV. Cells were then washed and incubated with antibodies against the surface markers CD3 (SK7, 1:10), CD57 (HNK-1, 1:20), and KLRG1 (SA231A2, 1:10) and with antibodies against the markers CD4 (RPA-T4, 1:20) and CD8 (SK1, 1:10) for the T cell panel, or CD56 (5.1H11, 1:20) and CD16 (3G8, 1:10) for the NK cell panel (all from BioLegend), in the presence of an Fc receptor–binding inhibitor antibody (Thermo Fisher). Cells were washed, fixed, and permeabilized using the Cytofix/Cytoperm kit (BD Biosciences) and 4% paraformaldehyde and intracellularly stained with antibodies against TNF-α (MAb11, 1:20), IFN-γ (B27, 1:20; both from BD Biosciences), granzyme B (GB11, 1:20), and perforin 1 (Dg9, 1:20; both from BioLegend). Samples were acquired with a BD Fortessa (BD Biosciences), and the cell populations were analyzed using FlowJo software (version 10.7.1). All experiments included single-stained controls performed at MD Anderson's South Campus Flow Cytometry and Cellular Imaging Facility.

Degranulation assays

NK cells were isolated from BM MNCs by negative magnetic selection. Cells were cultured using a mix of Click's and RPMI media (1:1) and stimulated with K562 cells (1:1 E:T) for 2 h at 37 °C and 5% CO_2. After incubation, cells were harvested, washed, and stained with Zombie UV. Cells were washed and incubated with antibodies against the surface markers CD3 (SK7, 1:10), CD56 (5.1H11, 1:20), CD16 (3G8, 1:10), CD57 (HNK-1, 1:20), CD107a (UCHL1, 1:20), NKG2D (1D11, 1:10), NCR3 (P30-15, 1:20; all from BioLegend), and NKG7 (polyclonal, 1:10; Epigentek) in the presence of an Fc receptor-binding inhibitor antibody (Thermo Fisher). Cells were acquired with a BD Fortessa (BD Biosciences) as described above.

Cytolysis assays

NK cells were isolated from BM MNCs by negative magnetic selection using the NK Cell Isolation Kit (Miltenyi Biotec). A fraction of the cells was expanded for 1 week with irradiated (100 Gy) K562-based feeder cells at a 2:1 feeder cell:NK cell ratio in the presence of recombinant human IL-2 (Proleukin, 200 U/mL; Chiron) in complete NK cell medium (RPMI/Clicks; CellGenix GmbH) on day 0. Freshly isolated or expanded NK cells were co-cultured in 96-well plates at a 1:2 E:T ratio with K562, THP-1, or MOLM-14 tumor targets pre-labeled with 2 mM green dye (CFSE, FITC; Thermo Fisher) in complete NK cell medium. Each well contained 30×10^3 tumor cells and 15×10^3 NK cells. Wells containing tumor-alone groups served as negative controls. Cells were incubated in an IncuCyte S3 live-cell analysis system (Sartorius). Frames were captured over time at 2 h intervals from four separate $1.75 \times 1.29\ mm^2$ regions per well with a 10x objective. Values from all four areas of each well were pooled and averaged across experimental duplicate wells. Results were expressed graphically as the percent normalized green object counts (live cells) over time.

scDNA-seq with antibody-oligonucleotide conjugates

Single-cell library DNA was prepared using the Tapestri Platform and reagents according to the manufacturer's protocol (MissionBio). Briefly, cryopreserved BM or PB MNCs were thawed, washed with RPMI-1640 medium supplemented with 40% FBS, 1% bovine serum albumin, and 5 mM EDTA, and counted using a Countess cell counter (Invitrogen). MNCs were normalized to 25,000 cells/μL in 40 μL and incubated with Human TruStain FcX (BioLegend) blocking buffer. Next, cells were stained with TotalSeq-D Human Heme Oncology Cocktail (BioLegend). Following staining, cells were washed in wash buffer and loaded onto the Tapestri instrument for single-cell encapsulation, lysis, and barcoding with 2 μmol/L antibody tag forward primer. DNA from barcoded cells was amplified via multiplex PCR using a targeted myeloid panel that included 279 amplicons across 37 genes associated with myeloid malignancies (https://designer.missionbio.com/catalogpanels/Myeloid-MDACC). DNA libraries were extracted from the droplets, followed by purification with Ampure XP beads (Beckman Coulter). Purified DNA libraries were indexed and sequenced on Illumina's NovaSeq 6000 SP with 250-bp paired-end multiplexed runs. Protein PCR products in the supernatant from the Ampure XP bead purification step were isolated by a 5 min incubation with 2 μL of 5′ biotin oligo. Isolated proteins were washed, and protein libraries were generated using a library template and i5/i7 indices via PCR. The protein library PCR product was cleaned again using Ampure XP beads. Protein libraries were quantified, quality-checked, and sequenced on Illumina's NovaSeq 6000 S4 with 150-bp paired-end multiplexed runs.

FASTQ files generated by the sequencer were processed using the Tapestri Pipeline V2, which included adapter trimming and sequence alignment (using Burrows-Wheeler Aligner) to the human genome (GRCh37/hg19), barcode correction, and cell find. We performed variant calling and genotyping as previously described[62]. The resulting DNA and protein data were analyzed using Mission Bio's Python-based Mosaic library (version 1.8). For DNA analysis, only a whitelist of manually reviewed, bona-fide somatic variants was loaded for further analysis. To filter out low-quality variants, we applied 'filter_variants' with the following parameters: min_dp = 5, min_gq = 0, min_vaf = 21, min_prct_cells = 0, min_mut_prct_cells = 0, min_std = 0. The AOC readouts were subjected to normalization, dimensionality reduction, and clustering for protein analysis to facilitate cell type identification in each sample. Normalization was performed using the centered logratio method with 'normalize_reads' (method = 'CLR') followed by dimensionality reduction with 'run_pca' (components = 10) and 'run_umap' (attribute = 'pca', n_neighbors = 20, metric = 'cosine', min_dist =). Subsequently, the transformed counts were clustered using 'cluster' (attribute = 'umap', method = 'graph-community'), employing the Louvain algorithm. Individual cell types were annotated by manually reviewing the patterns of specific cell surface markers in each cluster. For example, CD8+ T cells were identified based on CD3 and CD8 positivity, CD4+ T cells on CD3 and CD4 positivity, NK cells on CD16 and CD56 positivity, B cells on CD19 and CD22 positivity, conventional dendritic cells on CD1c and CD11c positivity, plasmacytoid dendritic cells on CD123 and CD303 positivity, and myelomonocytic cells on CD33, CD14, and CD64 positivity (Fig. 3A). The heatmap in Fig. 3A was generated using the ComplexHeatmap[63] package in R.

CRISPR/Cas9 gene editing of *DNMT3A* and *TET2*

We used two single-guide RNAs (sgRNAs) targeting human *DNMT3A*: crRNA1, TGGCGCTCCTCCTTGCCACG; crRNA2, GGGGACTTGGAGATCACCGC; and one targeting human *TET2*: crRNA, TTGTAGCCAGAGGTTCTGTC (Integrated DNA Technologies Inc). Cas9 protein (PNA Bio) and sgRNAs were incubated at room temperature for 15 min in a 3:1 reaction (15 μg Cas9 and 5000 ng sgRNAs). Alt-R HiFi Cas9 Nuclease 3-NLS (Integrated DNA Technologies) was used to form ribonucleoprotein pre-complexes with the sgRNAs.

Cord blood NK cells were expanded as previously described[55]. On day 7 of NK cell expansion, 1×10^6 NK cells were electroporated with 62 µM HiFi Cas9 alone or with ribonucleoprotein pre-complexes containing either *TET2* or *DNMT3A* sgRNAs using the Neon transfection system (Thermo Fisher) at three 10-ms pulses of 1600 V each. Following the electroporation, NK cells were co-cultured with 2×10^6 uAPC feeder cells at a 1:2 ratio (NK:uAPC) in Stem Cell Growth Medium (CellGenix GmbH) with 200 U/mL IL-2 and expanded for another 6 days. On day 13, NK cells were purified using NK negative selection with the NK Cell Isolation Kit (Miltenyi Biotec) for the cytolysis assays described above. The knockout (KO) efficiency of the genes was confirmed by Western blotting.

Western blotting

On day 13 of the gene editing experiment, 5×10^6 purified NK cells from control and *TET2*-KO or *DNMT3A*-KO groups were lysed using RIPA buffer supplemented with Halt protease and phosphatase inhibitor cocktail (Thermo Fisher). Protein lysates were collected after centrifugation at 18,000 g for 20 min at 4 °C. The total amount of protein was quantified using the Qubit Protein Assay Kit and a Qubit Fluorometer (Thermo Fisher). A total of 20 µg of protein was resolved by 4–12% Nu-PAGE gel (Thermo Fisher) by sodium dodecyl sulfate–polyacrylamide gel electrophoresis and electroblotted onto a polyvinylidene difluoride membrane. Membranes were blocked with a 5% non-fat milk Tris-buffered saline-Tween (TBS-T) solution and subsequently incubated with primary antibodies against DNMT3A (Thermo Fisher, #MA5-35334; 1:1000), TET2 (CST, #1895; 1:1000), and β-actin (CST, #5125; 1:2000) overnight at 4 °C. Secondary horseradish peroxidase–conjugated anti-mouse and anti-rabbit antibodies were incubated for 1 h at room temperature in 5% non-fat milk TBS-T. Enhanced chemiluminescence visualization was performed using the Super Signal West Dura extended duration substrate (Thermo Fisher). Densitometric quantitative comparison relative to β-actin was performed using Image J software (NIH) in three biological repeat samples.

Tumor rechallenge assays

Edited NK cells were subjected to multiple rounds of tumor challenges to determine the functional impact of TET2 or DNMT3A ablation in NK cells. Briefly, 1×10^5 NK cells from each condition were plated in poly-L-lysine–coated 48-well plates (Corning, #3548) with 5×10^4 GFP$^+$ THP-1 cells (2:1 E:T). Over time, NK cells' leukemic cell killing capacity was assessed in vitro using live imaging in an Incucyte SX5 (Sartorius). NK cells were rechallenged four additional times by adding fresh 5×10^4 THP-1 cells every 48–72 h. The percentage of live THP-1 cells was determined every 2 h over 10 days.

Bulk RNA-seq

Purified Cas9 control cells, *TET2*-KO NK cells, or *DNMT3A*-KO NK cells (1×10^6) were collected before the tumor challenge and after five tumor rechallenges. Following the fifth tumor challenge, 2×10^5 live NK (GFP$^-$CD45^{high}CD56$^+$CD16$^+$CD33$^-$CD123$^-$) cells were FACS-purified in an Aria II cell sorter (BD Biosciences). RNA was isolated using the RNeasy Mini kit (Qiagen), and 10 ng of total RNA was used for bulk small-input RNA sequencing. Illumina-compatible input mRNA libraries were prepared using the Smart-Seq V4 Ultra Low Input RNA kit (Takara Bio, USA) and the KAPA HyperPlus Library Preparation kit (Roche). Full-length double-stranded cDNA was generated from 10 ng of total RNA using Takara's SMART (Switching Mechanism at 5' End of RNA Template) technology, as previously described[64]. The double-stranded cDNA was amplified by five cycles of LD-PCR and then purified using Ampure Beads (Agencourt). Following bead elution, the cDNA was evaluated for size distribution and quantity using 4200 TapeStation High Sensitivity D1000 ScreenTape (Agilent Technologies) and Qubit dsDNA HS Assay Kits (Thermo Fisher), respectively. The cDNA was enzymatically fragmented, and 10 ng of the fragmented cDNA was used to generate Illumina-compatible libraries using the KAPA HyperPlus Library Preparation kit. The KAPA libraries were purified and enriched with eight cycles of PCR to create the final cDNA library. The libraries were assessed for size distribution using the Agilent Tapestation and quantified using the Qubit dsDNA HS Assay (Thermo Fisher). Equimolar quantities of 33 libraries were combined to create the final library pool. The pooled library was quantified by qPCR using the KAPA Library Quantification Kit (KAPA Biosystems), assessed for size distribution using the TapeStation 4200 (Agilent Technologies), and then sequenced on the Illumina NovaSeq 6000 SP flow cell using the 100 nt paired end-run format.

Bulk ATAC-seq analysis

ATAC-seq library preparation was performed at MD Anderson's Epigenomics Profiling Core with some modifications as previously described[65]. The nuclei were isolated from Cas9 control cells or *TET2*- or *DNMT3A*-KO NK cells after 5 challenges with the AML cell line THP-1. The nuclei were subjected to tagmentation using Tagment DNA enzyme (Illumina), followed by library preparation and DNA cleanup using SPRISelect beads (Beckman Coulter). Libraries were sequenced on an Illumina NovaSeq 6000 system to obtain at least 40 million high-quality mapping reads per sample. Paired-end sequencing reads were aligned to the hg38 reference genome using Bowtie2 (v2.4.2). Alignments were converted to BAM format, sorted, and indexed using samtools (v1.15). Mitochondrial reads were excluded using samtools, followed by removal of multi-mapped reads. Blacklisted genomic regions (ENCODE hg38 blacklist) were filtered using bedtools (v2.30.0). The resulting BAM files were re-sorted and indexed. For ATAC-seq peak calling, MACS2 (v2.2.9.1) was employed. Peaks from all samples were concatenated and merged using bedtools merge, and read counts per peak were quantified using bedtools multicov. Peak counts from each sample were combined to generate a peak matrix (with rows as peak regions and columns as samples) using R v4.1.0. The R package DESeq2 (v1.34.0) was used to find significantly different peaks across the treated and control samples. Peaks with an FDR < 0.05 were defined as significant peaks. Genes associated with the significant peaks were identified and annotated using the R package ChIPseeker (v1.30.3). Enriched motifs based on the significant peaks were predicted using the HOMER (v5.0.1) function findMotifsGenome. Fimo from the meme suite (v5.5.2) was used to identify peaks with specific TF binding motifs.

Mouse experiments

Mice were maintained under specific-pathogen-free conditions at MD Anderson and housed in a barrier facility at 25 °C under ambient oxygen conditions in a 12 h light/12 h dark cycle under 50% humidity, as previously described[1]. All animal experiments were performed with the approval of MD Anderson's Institutional Animal Care and Use Committee. NSGS mice were obtained from The Jackson Laboratory, and MISTRG mice were obtained from Regeneron.

Briefly, 2 month-old recipient NSGS mice were sublethally irradiated with a single dose of 2.6 Gy and then injected via the tail vein with a single-cell suspension containing 0.5×10^6 MDS-L cells. Human chimerism was analyzed after 4 weeks in BM aspirates by staining the mouse BM suspensions with antibodies against mouse CD45 (30-F11, 1:20; BioLegend) and human CD45 (HI30, 1:10; BD Biosciences). When human cells were first detected above a minimum confidence level (1%), mice with similar mean chimerism were randomized and injected with HD-derived NK cells previously edited using the CRISPR/Cas9 strategy to achieve *DNMT3A* or *TET2* depletion. Mice injected with HD NK cells transfected with Cas9 alone were used as controls. Intraperitoneal injections of human IL-2 (10,000 units/mouse) were administered every 2–3 days to support these cells' function. Ten days after NK injection, PB samples were collected in EDTA-coated tubes, and complete blood counts were performed with an automated ABX

Pentra Hematology Analyzer (Horiba, Irvine, CA). Mice were sacrificed and autopsied, and their rear legs and spleens were resected for analysis. For BM and spleen flow cytometric analyses, femurs, and tibias, or spleens, were crushed in the presence of a 2% FBS/PBS solution, and the cell suspensions were passed through 30-μm pre-separation filters (Miltenyi Biotec). Red blood cells were eliminated from splenic samples using BD Lysing Buffer (BD Biosciences).

Newborn (1- to 3 day-old) MISTRG mice[38] were sublethally irradiated (2 doses of 150 cGy 4 h apart). CCUS BM MNCs were incubated with a murine anti-human CD3 antibody (Okt3; BioXCell) on ice for 30 min at a concentration of 1×10^6 cells/μg just before intrahepatic injection, as previously described[39]. Human chimerism was analyzed 4 weeks after transplantation by flow cytometry of human CD45^{+} cells in PB. Xenografts were divided into two groups. One week after NK cell injection, the mice were sacrificed, and BM and splenic cells were isolated and analyzed by flow cytometry to assess the frequencies of human CD45^{+}CD56^{-} cells.

All NSGS mice used in this study were female, as female recipients have been shown to yield better engraftment rates than male recipients, regardless of donor sex[66]. MISTRG pups were selected exclusively based on availability upon birth, as xenotransplant was performed before their sex was distinguishable. Additionally, previous studies have not shown significant sex-related differences in immune reconstitution or hematopoietic function in this model[39].

NGS
The frequency of mutant cells in vehicle-treated or HD NK cell–treated xenografts was evaluated by extracting genomic DNA from sorted human CD45^{+} cells and subjecting it to 81-gene target PCR-based sequencing using an NGS platform as described previously[54]. Testing was performed in a Clinical Laboratory Improvement Amendments–certified laboratory.

Statistical analysis
Statistics and graphical representations were performed using GraphPad (version 10.0, La Jolla, CA). Figure legends indicate the statistical tests used in each experiment. Statistical significance was represented as $*P < 0.05$, $**P < 0.01$, $***P < 0.001$, $****P < 0.0001$.

Reporting summary
Further information on research design is available in the Nature Portfolio Reporting Summary linked to this article.

Data availability
The datasets generated in this study using scDNA-seq, RNA-seq, long-read scRNA-seq, and ATAC-seq have been deposited under GSE276492, GSE276360, GSE276974, and GSE289476, respectively. Source data are provided in this paper. The remaining data are available within the article, supplementary information, or source data file. Source data are provided with this paper.

References

1. Ganan-Gomez, I. et al. Stem cell architecture drives myelodysplastic syndrome progression and predicts response to venetoclax-based therapy. *Nat. Med.* https://doi.org/10.1038/s41591-022-01696-4 (2022).
2. Malcovati, L. et al. Clinical significance of somatic mutation in unexplained blood cytopenia. *Blood* **129**, 3371–3378 (2017).
3. Steensma, D. P. et al. Clonal hematopoiesis of indeterminate potential and its distinction from myelodysplastic syndromes. *Blood* **126**, 9–16 (2015).
4. Osman, A. When are idiopathic and clonal cytopenias of unknown significance (ICUS or CCUS)? *Hematol. Am. Soc. Hematol. Edu. Prog.* **2021**, 399–404 (2021).
5. de Visser, K. E. & Joyce, J. A. The evolving tumor microenvironment: From cancer initiation to metastatic outgrowth. *Cancer Cell* **41**, 374–403 (2023).
6. Gonzalez, H., Hagerling, C. & Werb, Z. Roles of the immune system in cancer: from tumor initiation to metastatic progression. *Genes Dev.* **32**, 1267–1284 (2018).
7. Vinay, D. S. et al. Immune evasion in cancer: mechanistic basis and therapeutic strategies. *Sem. Cancer Biol.* **35**, S185–S198 (2015).
8. Ghorani, E., Swanton, C. & Quezada, S. A. Cancer cell-intrinsic mechanisms driving acquired immune tolerance. *Immunity* **56**, 2270–2295 (2023).
9. Boudreau, J. E. & Hsu, K. C. Natural killer cell education and the response to infection and cancer therapy: stay tuned. *Trends Immunol.* **39**, 222–239 (2018).
10. Hamarsheh, S., Groß, O., Brummer, T. & Zeiser, R. Immune modulatory effects of oncogenic KRAS in cancer. *Nat. Commun.* **11**, 5439 (2020).
11. Efremova, M., Vento-Tormo, M., Teichmann, S. A. & Vento-Tormo, R. CellPhoneDB: inferring cell-cell communication from combined expression of multi-subunit ligand-receptor complexes. *Nat. Protoc.* **15**, 1484–1506 (2020).
12. Kirchhammer, N. et al. NK cells with tissue-resident traits shape response to immunotherapy by inducing adaptive antitumor immunity. *Sci. Transl. Med.* **14**, eabm9043 (2022).
13. Allen, F. et al. CCL3 enhances antitumor immune priming in the lymph node via IFNγ with dependency on natural killer cells. *Front. Immunol.* **8**, 1390 (2017).
14. Jhunjhunwala, S., Hammer, C. & Delamarre, L. Antigen presentation in cancer: insights into tumour immunogenicity and immune evasion. *Nat. Rev. Cancer* **21**, 298–312 (2021).
15. David, B. A. & Kubes, P. Exploring the complex role of chemokines and chemoattractants in vivo on leukocyte dynamics. *Immunol. Rev.* **289**, 9–30 (2019).
16. Goodridge, J. P., Burian, A., Lee, N. & Geraghty, D. E. HLA-F and MHC class I open conformers are ligands for NK cell Ig-like receptors. *J. Immunol.* **191**, 3553–3562 (2013).
17. Bogunia-Kubik, K. & Łacina, P. Non-KIR NK cell receptors: Role in transplantation of allogeneic haematopoietic stem cells. *Int. J. Immunogenet.* **48**, 157–171 (2021).
18. McNerney, M. E., Guzior, D. & Kumar, V. 2B4 (CD244)-CD48 interactions provide a novel MHC class I-independent system for NK-cell self-tolerance in mice. *Blood* **106**, 1337–1340 (2005).
19. Wu, Y. et al. Monocyte/macrophage-elicited natural killer cell dysfunction in hepatocellular carcinoma is mediated by CD48/2B4 interactions. *Hepatology* **57**, 1107–1116 (2013).
20. Pahima, H., Puzzovio, P. G. & Levi-Schaffer, F. 2B4 and CD48: a powerful couple of the immune system. *Clin. Immunol.* **204**, 64–68 (2019).
21. Batlle, E. & Massagué, J. Transforming growth factor-β signaling in immunity and cancer. *Immunity* **50**, 924–940 (2019).
22. Chang, J. T., Wherry, E. J. & Goldrath, A. W. Molecular regulation of effector and memory T cell differentiation. *Nat. Immunol.* **15**, 1104–1115 (2014).
23. Delpoux, A., Lai, C. Y., Hedrick, S. M. & Doedens, A. L. FOXO1 opposition of CD8(+) T cell effector programming confers early memory properties and phenotypic diversity. *Proc Natl Acad. Sci. USA* **114**, E8865–e8874 (2017).
24. Delpoux, A. et al. FOXO1 constrains activation and regulates senescence in CD8 T cells. *Cell Rep.* **34**, 108674 (2021).
25. Delpoux, A. et al. Continuous activity of Foxo1 is required to prevent anergy and maintain the memory state of CD8(+) T cells. *J. Exp. Med.* **215**, 575–594 (2018).
26. Crinier, A. et al. Single-cell profiling reveals the trajectories of natural killer cell differentiation in bone marrow and a stress signature

induced by acute myeloid leukemia. *Cell Mol. Immunol.* **18**, 1290–1304 (2021).

27. Donnelly, R. P. et al. mTORC1-dependent metabolic reprogramming is a prerequisite for NK cell effector function. *J. Immunol.* **193**, 4477–4484 (2014).

28. Loftus, R. M. et al. Amino acid-dependent cMyc expression is essential for NK cell metabolic and functional responses in mice. *Nat. Commun.* **9**, 2341 (2018).

29. Ramírez-Labrada, A. et al. All about (NK Cell-Mediated) death in two acts and an unexpected encore: initiation, execution and activation of adaptive Immunity. *Front. Immunol.* **13**, 896228 (2022).

30. Bryceson, Y. T., March, M. E., Barber, D. F., Ljunggren, H. G. & Long, E. O. Cytolytic granule polarization and degranulation controlled by different receptors in resting NK cells. *J. Exp. Med.* **202**, 1001–1012 (2005).

31. Verron, Q. et al. NK cells integrate signals over large areas when building immune synapses but require local stimuli for degranulation. *Sci. Signal* **14**, eabe2740 (2021).

32. Coënon, L. & Villalba, M. From CD16a biology to antibody-dependent cell-mediated cytotoxicity improvement. *Front. Immunol.* **13**, 913215 (2022).

33. Ben-Shmuel, A., Sabag, B., Biber, G. & Barda-Saad, M. The role of the cytoskeleton in regulating the natural killer cell immune response in health and disease: from signaling dynamics to function. *Front. Cell Dev. Biolo.* **9**, 609532 (2021).

34. Bernard, E. et al. Molecular international prognostic scoring system for myelodysplastic syndromes. *NEJM Evid.* **1**, EVIDoa2200008 (2022).

35. Sakai, Y. et al. The Rac activator DOCK2 regulates natural killer cell-mediated cytotoxicity in mice through the lytic synapse formation. *Blood* **122**, 386–393 (2013).

36. Kumar, B. et al. BATF is a major driver of NK cell epigenetic reprogramming and dysfunction in AML. *Sci. Transl. Med.* **16**, eadp0004 (2024).

37. Zhang, Y. et al. Engraftment of chronic myelomonocytic leukemia cells in immunocompromised mice supports disease dependency on cytokines. *Blood Adv.* **1**, 972–979 (2017).

38. Rongvaux, A. et al. Development and function of human innate immune cells in a humanized mouse model. *Nat. Biotechnol.* **32**, 364–372 (2014).

39. Song, Y. et al. A highly efficient and faithful MDS patient-derived xenotransplantation model for pre-clinical studies. *Nat. Commun.* **10**, 366 (2019).

40. Xie, Z. et al. Risk prediction for clonal cytopenia: multicenter real-world evidence. *Blood* https://doi.org/10.1182/blood.2024024756 (2024).

41. Uzhachenko, R. V. & Shanker, A. CD8(+) T lymphocyte and NK cell network: circuitry in the cytotoxic domain of immunity. *Front. Immunol.* **10**, 1906 (2019).

42. Merino, A. M., Kim, H., Miller, J. S. & Cichocki, F. Unraveling exhaustion in adaptive and conventional NK cells. *J. Leukoc. Biol.* **108**, 1361–1368 (2020).

43. Boy, M. et al. Myelodysplastic Syndrome associated TET2 mutations affect NK cell function and genome methylation. *Nat. Commun.* **14**, 588 (2023).

44. Serrano, G. et al. Single-cell transcriptional profile of CD34+ hematopoietic progenitor cells from del(5q) myelodysplastic syndromes and impact of lenalidomide. *Nat. Commun.* **15**, 5272 (2024).

45. Fraietta, J. A. et al. Disruption of TET2 promotes the therapeutic efficacy of CD19-targeted T cells. *Nature* **558**, 307–312 (2018).

46. Prinzing, B. et al. Deleting DNMT3A in CAR T cells prevents exhaustion and enhances antitumor activity. *Sci. Tansl. Med.* **13**, eabh0272 (2021).

47. Rodriguez-Sevilla, J. J. & Colla, S. Inflammation in myelodysplastic syndrome pathogenesis. *Semin. Hematol.* https://doi.org/10.1053/j.seminhematol.2024.09.005 (2024).

48. Kaito, Y. & Imai, Y. Evolution of natural killer cell-targeted therapy for acute myeloid leukemia. *Int. J. Hematol.* **120**, 34–43 (2024).

49. Zhang, X., Yang, X., Ma, L., Zhang, Y. & Wei, J. Immune dysregulation and potential targeted therapy in myelodysplastic syndrome. *Ther. Adv. Hematol.* **14**, 20406207231183330 (2023).

50. Rodriguez-Sevilla, J. J. et al. Hematopoietic stem cells with granulo-monocytic differentiation state overcome venetoclax sensitivity in patients with myelodysplastic syndromes. *Nat. Commu.* **15**, 2428 (2024).

51. Pei, S. et al. Monocytic subclones confer resistance to venetoclax-based therapy in patients with acute Myeloid Leukemia. *Cancer Discov.* **10**, 536–551 (2020).

52. Liu, E. et al. Use of CAR-transduced natural killer cells in CD19-positive Lymphoid tumors. *The N. Engl. J. Med.* **382**, 545–553 (2020).

53. Marin, D. et al. Safety, efficacy and determinants of response of allogeneic CD19-specific CAR-NK cells in CD19(+) B cell tumors: a phase 1/2 trial. *Nat. Med.* **30**, 772–784 (2024).

54. Kanagal-Shamanna, R. et al. Principles of analytical validation of next-generation sequencing based mutational analysis for hematologic neoplasms in a CLIA-certified laboratory. *Expert Rev. Mol. Diagn.* **16**, 461–472 (2016).

55. Daher, M. et al. Targeting a cytokine checkpoint enhances the fitness of armored cord blood CAR-NK cells. *Blood* **137**, 624–636 (2021).

56. Ma, F. et al. Single-cell profiling of prurigo nodularis demonstrates immune-stromal crosstalk driving profibrotic responses and reversal with nemolizumab. *J. Allergy Clin. Immunol.* **153**, 146–160 (2024).

57. Hao, Y. et al. Integrated analysis of multimodal single-cell data. *Cell* **184**, 3573–3587.e3529 (2021).

58. Korsunsky, I. et al. Fast, sensitive and accurate integration of single-cell data with harmony. *Nat. Methods* **16**, 1289–1296 (2019).

59. Zhou, Y. et al. Metascape provides a biologist-oriented resource for the analysis of systems-level datasets. *Nat. Commun.* **10**, 1523 (2019).

60. Gulati, G. S. et al. Single-cell transcriptional diversity is a hallmark of developmental potential. *Science* **367**, 405–411 (2020).

61. Billi, A. C. et al. Nonlesional lupus skin contributes to inflammatory education of myeloid cells and primes for cutaneous inflammation. *Sci. Transl. Med.* **14**, eabn2263 (2022).

62. Morita, K. et al. Clonal evolution of acute myeloid leukemia revealed by high-throughput single-cell genomics. *Nat. Commun.* **11**, 5327 (2020).

63. Gu, Z., Eils, R. & Schlesner, M. Complex heatmaps reveal patterns and correlations in multidimensional genomic data. *Bioinformatics* **32**, 2847–2849 (2016).

64. Terranova, C. J. et al. Reprogramming of H3K9bhb at regulatory elements is a key feature of fasting in the small intestine. *Cell Rep.* **37**, 110044 (2021).

65. Shah, V. V. et al. Mammary-specific expression of Trim24 establishes a mouse model of human metaplastic breast cancer. *Nat. Commun.* **12**, 5389 (2021).

66. Mian, S. A. et al. Influence of donor-recipient sex on engraftment of normal and leukemia stem cells in xenotransplantation. *Hemasphere* **8**, e80 (2024).

Acknowledgements

Author contributions

Competing interests

All authors declare no competing interests relative to this work.

Additional information

Supplementary information The online version contains supplementary material available at https://doi.org/10.1038/s41467-025-58662-0.

Correspondence and requests for materials should be addressed to May Daher or Simona Colla.

Reprints and permissions information is available at http://www.nature.com/reprints

Juan Jose Rodriguez-Sevilla[1,16], Irene Ganan-Gomez[1,16], Bijender Kumar[2,16], Natthakan Thongon[1], Feiyang Ma[3], Kelly S. Chien[1], Yi J. Kim[4], Hui Yang[1], Sanam Loghavi[5], Roselyn Tan[6], Vera Adema[1], Zongrui Li[4], Tomoyuki Tanaka[4], Hidetaka Uryu[4], Rashmi Kanagal-Shamanna[5], Gheath Al-Atrash[2], Rafael Bejar[6], Pinaki Prosad Banerjee[2], Sophia Lynn Cha[2], Guillermo Montalban-Bravo[1], Max Dougherty[7,8], Maria Claudina Fernandez Laurita[7,8], Noelle Wheeler[7,8], Baosen Jia[7,8], Eirini P. Papapetrou[7,8], Franco Izzo[7,8], Daniela E. Dueñas[9], Salome McAllen[9], Yiqian Gu[10], Gabriele Todisco[11,12], Francesca Ficara[12,13], Matteo Giovanni Della Porta[11,12], Abhinav Jain[14], Koichi Takahashi[1,4], Karen Clise-Dwyer[2], Stephanie Halene[15], Maria Teresa Sabrina Bertilaccio[1], Guillermo Garcia-Manero[1], May Daher[2] ✉ & Simona Colla[1] ✉

[1]Department of Leukemia, The University of MD Anderson Cancer Center, Houston, TX, USA. [2]Department of Stem Cell Transplantation and Cellular Therapy, The University of Texas MD Anderson Cancer Center, Houston, TX, USA. [3]Department of Cell and Developmental Biology, Feinberg School of Medicine, Northwestern University, Chicago, IL, USA. [4]Department of Genomic Medicine, The University of MD Anderson Cancer Center, Houston, TX, USA. [5]Department of Hematopathology, The University of Texas MD Anderson Cancer Center, Houston, TX, USA. [6]Moores Cancer Center, University of California San Diego, Moores Cancer Center, San Diego, CA, USA. [7]Department of Oncological Sciences, Icahn School of Medicine at Mount Sinai, New York, NY, USA. [8]Center for Advancement of Blood Cancer Therapies, Icahn School of Medicine at Mount Sinai, New York, NY, USA. [9]Department of Translational Molecular Pathology, The University of Texas MD Anderson Cancer Center, Houston, TX, USA. [10]Bioinformatics Interdepartmental Program, University of California Los Angeles, Los Angeles, CA, USA. [11]Department of Biomedical Sciences, Humanitas University, 20072 Pieve Emanuele Milan, Italy. [12]IRCCS Humanitas Research Hospital, 20089 Rozzano Milan, Italy. [13]Istituto di Ricerca Genetica e Biomedica, National Research Council, 20090 Milan, Italy. [14]Department of Epigenetics and Molecular Carcinogenesis, Center for Cancer Epigenetics, The University of MD Anderson Cancer Center, Houston, TX, USA. [15]Section of Hematology, Department of Internal Medicine and Yale Cancer Center, Yale University School of Medicine, New Haven, CT, USA. [16]These authors contributed equally: Juan Jose Rodriguez-Sevilla, Irene Ganan-Gomez, Bijender Kumar. ✉e-mail: mdaher@mdanderson.org; scolla@mdanderson.org